Structural Chemistry
https://doi.org/10.1007/s11224-024-02442-x

RESEARCH

Different topology of mixed valence $Co^{II}Co^{III}$ complexes with SCN anions and hydrazone–pyridine-based ligands

Ghodrat Mahmoudi[1,2,3] · Alexander S. Novikov[2,4,5] · Tomislav Balić[6] · Ennio Zangrando[7] · Jonathan M. White[8] · Bagher Eftekhari-Sis[1]

Received: 22 November 2024 / Accepted: 17 December 2024

Abstract

Two novel mixed valence $Co^{II}Co^{III}$ complexes $[Co_4^{II}(SCN)_{12}(EtOH)_2Co_4^{III}(L1)_8]$ (**1**) and $[Co^{II}(SCN)_2Co_2^{III}(L2)_4]_n$ (**2**) (HL1 = *N'*-(1-(pyridin-2-yl)ethylidene)nicotinohydrazide and HL2 = *N'*-(phenyl(pyridin-2-yl)methylene)isonicotinohydrazide) have been synthesized and structurally characterized by the single crystal X-ray crystallography. In both cases, the deprotonated ligands HL1 and HL2 behave as chelating species toward Co^{III}, further connecting Co^{II} fragments through the nicotine pyridine donors. A different topology is observed in the solid state of these complexes, complex **1** being an octanuclear cyclic species, while **2** is a 1D coordination polymer. The DFT calculations followed by the topological analysis of the electron density distribution have shown the existence of interesting non-covalent S···π-system interactions in **1**. The CSD database search for similar supramolecular motif involving NCS anion has shown that the number and strength of S···π interactions depend both on acidity of metal cation and number aromatic systems in the molecular structure of ligand.

Keywords Co(II, III) complexes · Mixed valence · Hydrazine-pyridine ligands · Octanuclear Co complex · Coordination polymer · S···π interactions

Introduction

Hydrazones represent an interesting group of organic compounds that have been extensively studied as biologically active molecules [1, 2], optical materials [3, 4], and sensors [5, 6]. They are typically formed by simple condensation reaction of appropriate hydrazine and carbonyl precursors. Some more recent investigations have shown that hydrazones can be easily synthesized not only by conventional solution-based syntheses but also by electrochemical [7], ultrasonic [8], mechanochemical [9], and photochemical [10] methods. Among these novel methods, mechanochemical synthesis is especially interesting due to the reduction of reaction time and excellent reaction yields [9, 11]. Hydrazones have also been widely used as a precursors for the synthesis of various biologically active substances [12–15]. The flexibility of hydrazone compounds and the presence of strong hydrogen donor (NH) and acceptor groups (C = O) make these compounds especially convenient for enzyme active site binding, and consequently inhibition and pharmaceutical application (e.g., xanthine oxidase [16]) Recent structural investigations of hydrazone derivatives have shown a significant binding affinity of these compounds to the MDM2 (Dalton's lymphoma) [17] and ARO (brest cancer)

✉ Ghodrat Mahmoudi
ghodratmahmoudi@gmail.com

1 Department of Chemistry, Faculty of Science, University of Maragheh, P.O. Box, Maragheh 55136-83111, Iran

2 Chemistry Department, Faculty of Engineering and Natural Sciences, Istinye University, Sarıyer, Istanbul 34396, Turkey

3 Department of Technical Sciences, Western Caspian University, Baku 1001, Azerbaijan

4 Saint Petersburg State University, Universitetskaya Nab., 7/9, Saint Petersburg 199034, Russian Federation

5 Peoples' Friendship University of Russia (RUDN University), Miklukho-Maklaya Street, 6, Moscow 117198, Russian Federation

6 Department of Chemistry, Josip Juraj Strossmayer University of Osijek, Cara Hadrijana 8/A, 31000 Osijek, Croatia

7 Department of Chemical and Pharmaceutical Sciences, University of Trieste, Via L. Giorgieri 1, 34127 Trieste, Italy

8 BIO-21 Molecular Science and Biotechnology, University of Melbourne, Parkville, Victoria 3052, Australia

Published online: 24 December 2024

[18] proteins. Hydrazones and their derivatives can act as ligands, forming a vast number of coordination compounds with transition metals [19–21]. The hydrazone group offers a versatile binding site through its *N*- and *O*-donor atoms, in most cases acting as a multidentate ligand. If a pyridine ring is present in the structure of the hydrazone derivative, the number of donor atoms and binding sites is increased, consequently enhancing the stability and chemical versatility of these compounds. Depending on the position of the pyridine nitrogen atom, these compounds can form discrete [22, 23], polymeric [24, 25], or polynuclear [26–28] coordination compounds. Discrete hydrazone-pyridine coordination compounds have recently attracted much attention due to their excellent antitumor activity [29–31]. Cu(II), Ru(III), and Pt(II) discrete complexes are among the most promising candidates for this application [32–34]. Hydrazone-pyridines can be variously mono- or bis-substituted by pyridine rings [35–37]. Regarding conformational aspects of these ligands, it is worth noting that in some instances *N*-donor atom of pyridine moiety can be oriented toward *N*,*O*-donor binding site (*endo*-oriented), or outwards (*exo*-oriented). In bis-pyridine derivatives, a mixed *endo-exo* orientation is possible, which usually leads toward the formation of chelated polymeric structures in which one *N*-donor atom (*endo*-oriented) participates in the formation of chelate, and the other gives rise to polymeric structure [38–40]. Such mixed orientation of donor atoms can also result in the formation of oligomeric coordination compounds. This mixed form of coordination, typical for hydrazone-pyridines, has been exploited for the preparation of [$n \times n$] polynuclear grids with Cu(II), Co(II), and Fe(II) ions [41] (*n* represents the number of possible coordination pockets in the structure of a ligand). If all conditions are met in the synthesis of these polynuclear compounds, a mixed valence state of metal ions can be achieved. There are a few examples of Fe(II, III) and Co(II, III) mixed valence compounds with hydrazone-pyridines, displaying interesting redox, catalytical, and magnetic properties [42, 43].

Herein, we present the structural characterization of two novel mixed valence Co(II, III) coordination compounds (**1**, **2**) with *N'*-(1-(pyridin-2-yl)ethylidene)nicotinohydrazide (HL1), and *N'*-(phenyl(pyridin-2-yl)methylene)isonicotinohydrazide (HL2). The molecular and crystal structure of both compounds was determined by single-crystal X-ray diffraction that revealed a different topology in solid state, namely a discrete octanuclear complex for **1** and a 1D polymeric chain for **2**.

Experimental section

Materials and methods

All reagents and solvents used for synthesis and analysis were commercially available and used as received. Acetylpyridine and nicotinic acid hydrazide were supplied from Sigma-Aldrich; isonicotinic acid hydrazide and phenyl-2-pyridyl ketone were supplied from Merck. FTIR spectra were recorded on a Bruker Tensor 27 FTIR spectrometer. Microanalyses were performed with a Heraeus CHN-O-Rapid analyzer.

X-ray crystallography

Diffraction data of compounds **1** and **2** were collected at 100(2) K at MX2 Beamline Australian Synchrotron ($\lambda = 0.710755$ Å) and at room temperature on a Bruker D8 Venture Photon III-14 diffractometer using graphite monochromated Mo-K_α radiation ($\lambda = 0.71073$ Å). Data reductions were performed with XDS [44] and APEX3 [45] software packages, respectively, and proper absorption corrections were applied to the data sets [46]. The structures were solved by direct methods with the program SHELXL-2019/2 [47] and refined by full-matrix least-squares procedures using the SHELXTL program [47]. The hydrogen atoms were placed at calculated positions and constrained to ride to atoms to which they are attached, except that of ethanol oxygen in **1** which was located on the Fourier map and freely refined. The ethanol molecule in **1** presents two orientations of C atoms which were refined with occupancies of 0.539/0.461(7). The phenyl group of two ligands in **2** presents two different orientations, refined with occupancies of 0.716/0.284(13) and 0.612/0.388(10). Squeeze program [48] has been applied to data of **2** to consider highly disordered solvent molecules and anions. Drawings were done with Diamond 3.2 [49]. ORTEP drawings of asymmetric units of the structures are reported as supplementary material. The oxidation state of cobalt(II) and cobalt(III) in the compounds was confirmed by the bond valence analysis methodology [50]. Details of crystallographic data and refinements are given in Table S1.

Syntheses

Ligands were prepared by the method described in our previous paper [51] and used without further purification. Structures of ligands are presented in Scheme 1.

Preparation of HL1 = N'-(1-(pyridin-2-yl)ethylidene) nicotinohydrazide and HL2 = N'-(phenyl(pyridin-2-yl) methylene)isonicotinohydrazide

HL1 was prepared by mixing an ethanol (50 mL) solution of 2-acetylpyridine (1.214 g; 10 mmol) and nicotinic acid hydrazide (1.371 g;10 mmol) with the addition of 5 drops of CH_3COOH. The resulting solution was refluxed for 3 h in an oil bath. The volume of the reaction mixture was reduced using a rotary evaporator to about 15 mL white precipitate started to form. Insoluble product was removed

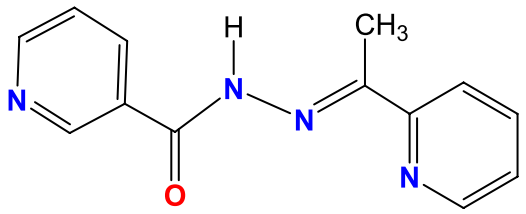

HL1

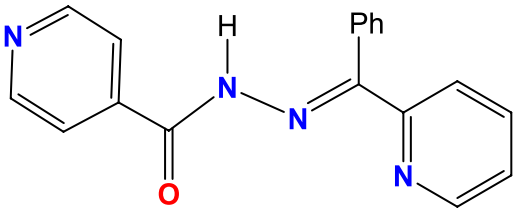

HL2

Scheme 1 Structure of ligands HL1 and HL2

by filtration, washed with ice-cold ethanol (3 × 2 mL), and dried on air to give pure product (1.92 g) with a yield of 80%. The same method was used for the preparation of HL2, except phenyl(pyridin-2-yl)methanone (1.832 g; 10 mmol) and isoniazid (1.371 g;10 mmol) were used as starting reagents yield for HL2: 2.7362 g (90%). HL1: Anal. Calc. for $C_{13}H_{12}N_4O$ (240.2) (%): C 64.99, H 5.03 and N 23.32; found: C 64.5, H 4.94 and N 24.01. IR data (KBr, cm^{-1}) ν: 3196 (NH), 3041 (Ar–CH), 2982 (Alip.-CH), 1669 (C = O), 1569 (CH = N), 1469, 1429 $(CH=N)_{pyridine}$. HL2: Anal. Calc. for $C_{12}H_{10}N_4O$ (302.34) (%): C 71.51, H 4.67, and N 18.53; found: C 71.51, H 4.51, and N 18.69. IR data (KBr, cm^{-1}) ν: 3365 (NH), 3063 (Ar–CH), 1689 (C = O), 1540 (CH = N), 1470, 1412 $(CH=N)_{pyridine}$.

Preparation of 1 and 2

Complex **1** was synthesized through the reaction of the organic ligand HL1 (0.024 g, 0.10 mmol) with $CoCl_2{\cdot}6H_2O$ (0.010 g, 0.10 mmol) and KSCN (0.065 g, 1.0 mmol) by a thermal-gradient method in a branched tube using ethanol (10 mL) as the solvent. The tube was sealed and immersed in an oil bath at 60 °C, and the branched arm was kept at ambient temperature. After 2 days, crystals of **1** formed in the cooler arm and were collected by filtration, washed with acetone and diethyl ether, and dried in air. For the preparation of complex **2**, HL2 was used instead of HL1 in the same molar ratio, using the described thermal-gradient method.

Computational details

The single-point DFT calculations based on the experimental X-ray geometry of **1** have been carried out at the ωB97XD/CEP-121G level of theory with the help of the Gaussian-09 [52] program package. The topological analysis of the electron density distribution (QTAIM analysis) was performed using the Multiwfn program (version 3.7) [53]. The Cartesian atomic coordinates for the model structure used for DFT calculations are presented in Table S2, Supporting Information.

Results and discussion

Crystal structures

Compound **1** crystallizes in triclinic space group $P\bar{1}$ and the X-ray structural analysis reveals a centrosymmetric cyclic octanuclear Co_8 complex shown in Fig. 1a built by four independent cobalt atoms. Both the Co^{III} metals (Co2 and Co3) are hexacoordinated in a distorted octahedral N_4O_2 coordination sphere by two pyridyl-imine moieties and two carbonyl oxygen atoms from two pincer-type chelating HL1 ligands. The Co–N bond lengths fall in the range 1.855(2)–1.930(2) Å, while the Co–O ones vary from 1.887(2) to 1.923(2) Å (Table S3). On the other hand, the divalent Co1 and Co4 show a different coordination environment. Co1 is five-coordinated by three terminal thiocyanate anions in the equatorial plane (Co1-NCS bond lengths average to 1.983 Å) and by two nicotinohydrazide pyridine donors as axial donors in the trigonal bipyramidal geometry, with Co1-N bond distances of 2.149(2) and 2.244(2) Å. On the other hand, Co4 exhibits a distorted octahedral geometry with an additional ethanol molecule coordinated. Here, the Co4-NCS and Co4-N(py) average to 2.066 and 2.158 Å, respectively, while the Co4-O(Et) is of 2.209(3) Å (Table S3). The described connections result in an octanuclear complex where metals Co2 and Co3 delineate the vertices of a distorted square of side 14.247 and 14.416 Å (Fig. 1b). In the crystal packing, the complexes weakly interact via π-stacking interactions involving pyridine rings referred by inversion center (Fig. S1) with centroid distance of 3.934(2) Å, and by H-bond O5-H5···S2 (at x, $1+y$, z) with O···S distance of 3.221(3) Å.

Inspection of the crystallographic data reveals the presence of unusual noncovalent interactions S···π-system in the X-ray structure of complex **1**. To understand the nature and quantify the strength of these intramolecular interactions, DFT calculations followed by the topological analysis of the electron density distribution within the QTAIM approach [54] were carried out at the ωB97XD/CEP-121G level of theory for model structure (see Computational details, Table S2, and the attached xyz-file in ESI). We carried out single-point calculations based on the experimentally obtained crystal structure and have not used fully relaxed geometry because we are interested in evaluating the interactions as they stand in the solid state instead of finding the most global minimum energy of the complex. This procedure has been previously used many times by

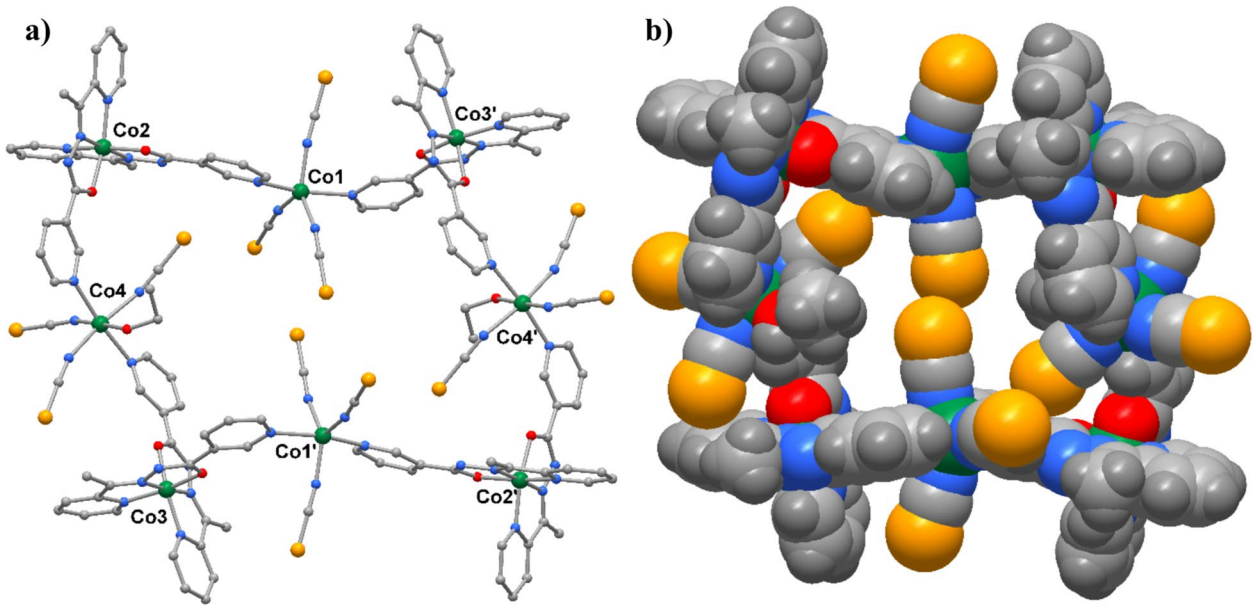

Fig. 1 **a** The molecular structure of the centrosymmetric octanuclear complex **1** (primed atoms at $-x+2, -y+1, -z+2$). **b** The correspondent space-filling representation

our group [55–59] and others [60–65] to investigate noncovalent interactions in the solid state. Results of QTAIM analysis are summarized in Table 1; the contour line diagram of the Laplacian of electron density distribution $\nabla^2\rho(\mathbf{r})$, bond paths, and selected zero-flux surfaces, visualization of electron localization function (ELF), and reduced density gradient (RDG) analyses for noncovalent interactions S···π-system in the X-ray structure of **1** is shown in Fig. 2a–2c.

** $E_{int} \approx -V(r)/2$[67]

The QTAIM analysis of model structure demonstrates the presence of bond critical point $(3,-1)$ for intramolecular interactions S···π-system (via one S···C contact 3.251 Å) in the X-ray structure of **1** (Table 1). The low magnitude of the electron density, positive value of the Laplacian of electron density, and very close to zero positive energy density in this bond critical point $(3,-1)$ and estimated strength for appropriate short contact are typical for weak noncovalent interactions involving chalcogen atoms in similar chemical systems [68–72]. The balance between the Lagrangian kinetic energy G(r) and potential energy density V(r) at the bond critical points $(3,-1)$ reveals the nature of these interactions, if the ratio $-G(r)/V(r) > 1$ is satisfied, then the nature of appropriate interaction is purely noncovalent, in case the where $-G(r)/V(r) < 1$, some covalent components take place [73]. Based on this criterion, one can state that a covalent contribution in intramolecular interactions S···π-system in the X-ray structure of **1** is absent. The Laplacian of electron density is typically decomposed into the sum of contributions along the three principal axes of maximal variation, giving the three eigenvalues of the Hessian matrix (λ_1, λ_2, and λ_3), and the sign of λ_2 can be utilized to distinguish bonding (attractive, $\lambda_2 < 0$) weak interactions from nonbonding ones (repulsive, $\lambda_2 > 0$) [74, 75]. Thus, all discussed intramolecular interactions S···π-system in the X-ray structure of **1** are attractive (Table 1).

These S···π interactions are a rare form of intermolecular contacts, usually observed in structures of proteins [76], where they play an important role in tertiary structure. In proteins, these interactions were predominantly found between neutral S-containing fragments of the protein (usually cysteine) and aromatic systems (phenylalanine, tyrosine, etc.). On the other hand, the NCS anion can also participate

Table 1 Values of the density of all electrons, ρ(r); Laplacian of electron density, $\nabla^2\rho(r)$; and appropriate λ_2 eigenvalue, energy density, H_b; potential energy density, V(r), and Lagrangian kinetic energy, G(r) (a.u.) at the bond critical point $(3,-1)$, corresponding to intramolecular interactions S···π-system in the molecular structure of **1**, and estimated strength for these interactions E_{int} (kcal/mol)

Contact*	% $_{vdw\ sum}$	ρ(**r**)	$\nabla^2\rho(\mathbf{r})$	λ_2	H_b	V(**r**)	G(**r**)	E_{int}**
S···C 3.251 Å	93%	0.011 a.u	0.034 a.u	−0.011 a.u	0.001 a.u	−0.006 a.u	0.007 a.u	1.9 kcal/mol

*The Bondi's (shortest) van der Waals radii for S and C atoms are 1.8 and 1.7 Å, respectively [66]

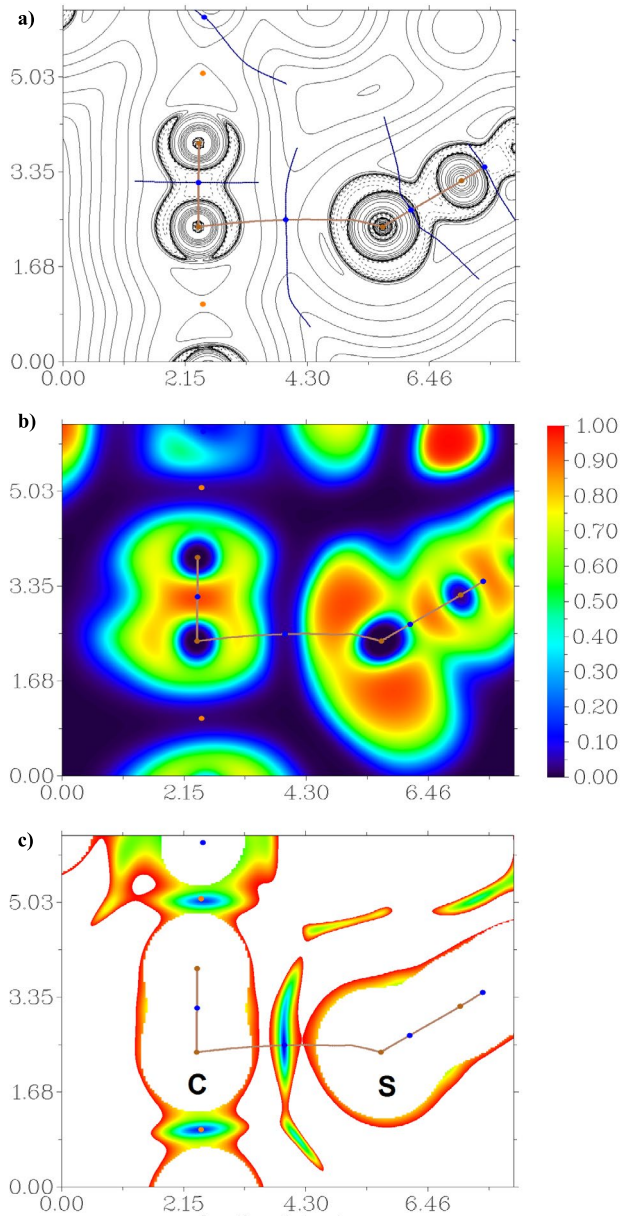

Fig. 2 **a** Contour line diagram of the Laplacian of electron density distribution $\nabla^2\rho(r)$, bond paths, and selected zero-flux surfaces. **b** Visualization of electron localization function (ELF). **c** Reduced density gradient (RDG) analyses for intramolecular interactions S···π-system in the molecular structure of **1**. Bond critical points (3, −1) are shown in blue, nuclear critical points (3, −3) in pale brown, ring critical points (3, +1) in orange, length units on the axes of calibration scale Å, and the color scale for the ELF and RDG maps is presented in a.u

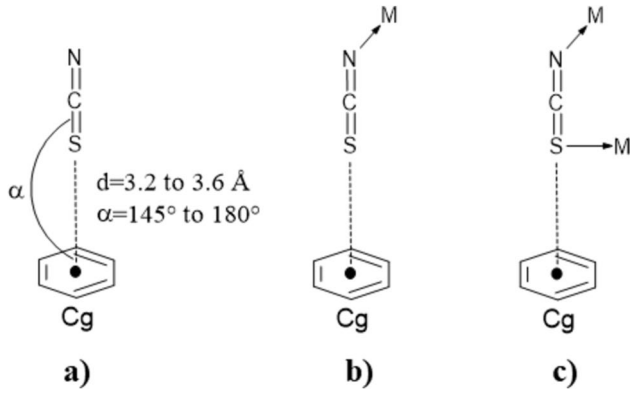

Fig. 3 **a** CSD database search parameters. **b** Terminal N-coordination mode of S···π interactions. **c** Bridging N, S-coordination mode of S···π interactions

in the S···π interactions, but unlike in proteins, this interaction can be classified as anion···π interaction. Most often anion···π interactions involve halide anions and haloarenes (e.g., hexafluorobenzene). The geometry of these simple anion···π interactions is "π-facial", with centroid-anion distances ranging from 3 to 5 Å, and energies up to 25 kcal/mol [77]. Polyatomic, complex anions can form a vast number of different anion···π interactions, depending on anion geometry, atom number, and chemical composition of the aromatic system. As an ambidentate ligand (molecule), NCS anion can form anion···π interactions through N or S atoms. A recent study [78] of a triazine macrocycle compound (tetraoxacalix[2]arene[2]triazine) as a host molecule for anions has shown that NCS anion can form anion···π interactions simultaneously using both N and S atoms. As reported by the authors, this type of interaction is weak, displaying a stability constant value 10^2 lower than for nitrate anion, thus implying that this type of interaction is not particularly important in supramolecular engineering nor anion recognition. Nevertheless, for compound **1** here reported, the NCS anions may be of importance in the formation of supramolecular motifs. Therefore, the CSD database [79] was searched for S···π interactions involving the NCS group and any type of aromatic system. The search was done for non-disordered structures, S···π (centroid) distance set from 3.2 to 3.6 Å, and C = S···Cg angle(α) from 145° to 180° (π-facial arrangement- Fig. 3a). Under these conditions, 152 relevant crystal structures were found with a mean S···π distance of 3.463 Å and C = S···Cg angle of 157.9°. Interestingly almost all compounds are built of coordinated nitrogen heterocyclic ligands, N-coordinated NCS anions, and metal cations (Fig. 3b). The search has also shown that two possible coordination modes of NCS anion result in the formation of S···π interactions: terminal N-coordinated (Fig. 3b) and bridging N, S-coordinated (Fig. 3c). It is important to emphasize that there are only 6 examples of S···π interactions with N, S-coordinated NCS (CSD codes: ABOVUL [80], ATEHUE [81], BOYQAH [82], FAXJUM [83], GIFGIN [84], ILETOI [85]), and all with soft metal cations (Hg(II), Ag(I), Cu(I)).

From the scatterplot of database search data analysis (Fig. S2), it can be seen that the S···π distance for most interactions are longer than 3.45 Å, and that the C = S···Cg

angles are in most compounds under 165° (offset π-facial). Ideally, to realize a strong S···π interaction, distance should be as short as possible (off course not so short to create strong repulsive interactions) and angles should be close to 180°. Interestingly, shorter and high-angle S···π interactions were found among discrete complex compounds composed of hard acid cations (Fe(III) – QUNYEE [86], Mn(II) – BOFNAN [87], Cr(III) – HAXXEL [88]) and N-polyaromatic ligands. Such occurrence could be interpreted by electron-withdrawing effect of coordinated metal cation that induces favorable electronic state of S atoms for the formation of S···π interactions. Likewise, the ligands in the abovementioned compounds contain up to 3 fused aromatic rings (e.g., 1,10-phenanthroline), which definitely increase the probability of favorable S···π contacts. Based on CSD database search, it can be concluded that the number and strength of S···π interactions depend on both effects, i.e., acidity of metal cation and number of aromatic systems in the ligand.

The structural determination of complex **2** discloses a 1D square-type open microporous material, consisting of infinite chains elongated in the direction of the crystallographic [1 −1 0] direction (Fig. 4a). Compound **2** also crystallizes in triclinic space group $P\,\bar{1}$ with three independent Co atoms, all having a distorted octahedral geometry. Co2 and Co3 are doubly chelated by two deprotonated ligands HL2 meridional orientated through the pyridyl and imine nitrogen donors and the carbonyl oxygen atom (Fig. S3). The Co–N and Co–O bond distances vary between 1.844(3)−1.928(4) and 1.899(3) 1.926(3) Å, respectively, following a similar trend as observed in **1** (Table S4). Then, the pyridine nitrogen of the isonicotinohydrazide ligands coordinate the $Co1(NCS)_2$ fragments of divalent cobalt (Fig. S3), with Co1-N(py) = 2.171(3)–2.215(3) Å, while Co1-NCS is of 2.056(4) Å (mean value). This mode of coordination produces an infinite 1D coordination polymer structure displaying a looped chain motif (Fig. 4b). The presence of the bulky phenyl group and the position of the pyridine N in isonicotinohydrazide ligands give rise to a 1D loop chain sharing the cobalt(II) node Co1 and with side metal–metal distance within the loop of ca. 8.95 Å.

The final question regarding the structural features of these complexes is related to the potential control of supramolecular aggregation. As reported, both compounds were prepared under an identical synthetic procedure using the same metal cation and anions source. Under these conditions, **1** forms a polynuclear species, while **2** is a polymeric species. Although NCS anion can be of an importance in supramolecular aggregation (above-described examples of S···π interactions), most often topological differences arise due to bridging ability of this anion. Therefore, different topologies in **1** and **2** must be related to the molecular

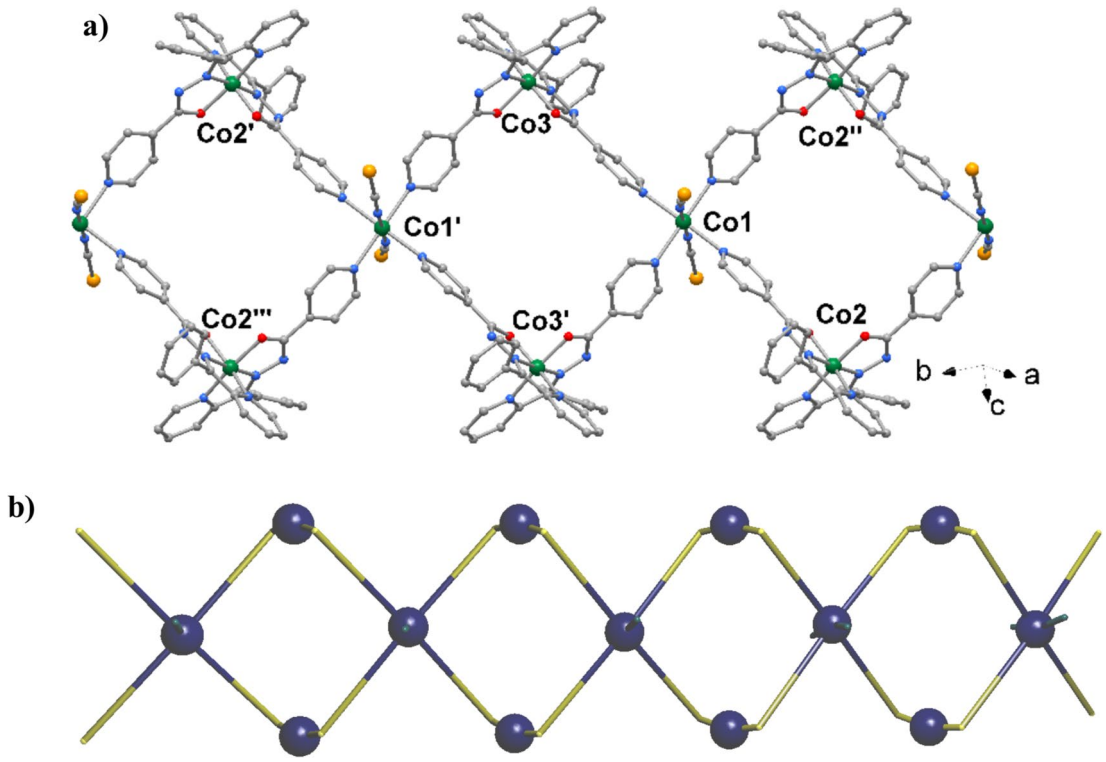

Fig. 4 **a** The polymeric chain of compound **2** (H atoms not shown for clarity). **b** Schematic representation of 1D *looped chain* (blue spheres are metal ions, yellow tubes ligand, and teal tubes anion fragments)

structure of ligands (HL1 and HL2) since other reactants used in synthesis are identical. Interestingly in both compounds, Co(III) ions are coordinated by two mutually orthogonal ligands (angles between pyridine moieties are of 76.82° and 75.28° in **1** and **2**, respectively) resulting in the predefined geometry of chelated species. In **1**, N-atom on pyridine substituent is in meta position (nicotinohydrazide moieties), which geometrically favors the coordination of two adjacent pyridine moieties to Co(II) ion, consequently resulting in the formation of polynuclear species. Unlike in **1**, in complex **2** N-atoms on the pyridine substituent are in the *para* position (isonicotinohydrazide), which favors coordination of 4 adjacent chelated species resulting in the formation of polymeric species. It is also noteworthy to mention that the presence of bulky phenyl moieties in HL2 is probably the reason why only low-dimensional coordination polymer (1D) is formed in the case of compound **2**, and not high-dimensional polymers or MOFs (2D and 3D). Considering the potential control over supramolecular aggregation in this group of compounds, one can make a reasonable set of guidelines: (i) Co(III) prefer chelated coordination environment, while Co(II) ions are flexible in this sense; (ii) polynuclear species are likely to form when N-donor atoms of adjacent pyridine groups are close to the chelated species; and (iii) polymeric species will likely form when N-donor atom of adjacent pyridine groups are essentially at the opposite side of chelated species. A similar approach for the formation of coordination polymers and polynuclear complexes was previously reported for chelated macrocyclic ligands, usually used for the preparation of 3D motifs like MOFs. [89]

FT-IR spectroscopy

FT-IR spectra of both ligands are rather similar. In both spectra, very strong maxima close to 1660 cm^{-1} are due to the stretching vibration of the C = O group. Maxima close to 3100 and 1100 cm^{-1} can be attributed to the hydrazide group's N–H and N–N stretching vibration, respectively. Vibrations close to 1550 cm^{-1} in both spectra can be assigned to C = N stretching vibrations of pyridine rings. Compared to the spectrum of uncoordinated ligand HL1, the spectrum of complex **1** shows a very strong maximum at 2053 cm^{-1} (Fig. S4), which is typical for the C = N stretching vibration of the N-coordinated NCS anion [90]. In addition, the spectrum of complex N–H stretching and vibration of the hydrazide group is not present indicating that the ligand is in the deprotonated form. Both C = O and C = N stretching vibrations are red-shifted indicating participation of these groups in the coordinative bonding. The spectrum of complex **2** (Fig. S5) is almost identical, indicating a similar coordination mode of ligand HL2 and thiocyanate anion to the Co ions.

Conclusions

The two novel mixed valence $Co^{II}Co^{III}$ complexes (**1** and **2**) have been prepared and structurally characterized. Complex **1** forms an octanuclear cyclic species, while complex **2** exhibits a 1D coordination polymeric structure. In both compounds, Co(III) ions are coordinated by two deprotonated ligands in a distorted octahedral N_4O_2 coordination geometry. Co(II) ions are connected to the nicotine pyridine moiety of such formed chelated species, resulting in the formation of polynuclear (**1**) or polymeric (**2**) structures. NCS anions are coordinated to Co(II) ions and act as terminal ligands. The DFT calculations and topology analysis of electron density distribution highlight the presence of unusual non-covalent S···π interactions in **1**. It was also found that the number and strength of S···π interactions depend on the acidity of metal cation and number of aromatic systems in the molecular structure of ligand. The herein-presented findings are important in understanding the relationship between the topology of specific materials and the molecular structure of ligand species.

Supplementary information The online version contains supplementary material available at https://doi.org/10.1007/s11224-024-02442-x.

Acknowledgements The DFT calculations and topological analysis of the electron density distribution were supported by the RUDN University Scientific Projects Grant System, project № 021342-2-000.

Author contribution G. M.: Conceptualization, Data curation, Writing-Reviewing and Editing, Investigation, Formal analysis. A. S. N.: Writing- Original draft preparation, Data curation, Writing- Reviewing and Editing. T. B.: Writing- Original draft preparation, Writing- Reviewing and Editing. E. Z.: Writing- Reviewing and Editing, Formal analysis, Investigation. J. M. W.: Writing- Original draft preparation, Formal analysis, Investigation. B. E.-S.: Methodology, Writing- Original draft preparation, Writing- Reviewing and Editing, Formal analysis.

Funding The DFT calculations and topological analysis of the electron density distribution were supported by the RUDN University Scientific Projects Grant System, project № 021342–2-000.

Data availability No datasets were generated or analysed during the current study.

Declarations

Competing interests The authors declare no competing interests.

References

1. Kool ET, Crisalli P, Chan KM (2014) Org Lett 16:1454–1457
2. Kölmel DK, Kool ET (2017) Chem Rev 117:10358–10376
3. Meenatchi V, Han SS (2022) J Mol Struct 1270:133997
4. Rawat P, Singh RN, Gautam A, Kumar M, Singh R, Bharati P (2022) ACS Omega 7:29571–29586

5. Sousa RPCL, Teixeira F, Costa SPG, Figueira RB, Raposo MMM (2024) Dyes Pigm 225:112053
6. Chen W, Liang H, Wen X, Li Z, Xiong H, Tian Q, Yan M, Tan Y, Royal G (2022) Inorg Chim Acta 532:120760
7. Song S, Shi X, Zhu Y, Ren Q, Zhou P, Zhou J, Li J (2022) J Org Chem 87:4764–4776
8. Khalid M, Ali A, Abid S, Tahir MN, Khan MU, Ashfaq M, Imran M, Ahmad A (2020) ChemistrySelect 5:14844–14856
9. Pisk J, Đilović I, Hrenar T, Cvijanović D, Pavlović G, Vrdoljak V (2020) RSC Adv 10:38566–38577
10. Kushwaha AK, Maury SK, Kamal A, Singh HK, Pandey S, Singh S (2023) Chem Commun 59:4075–4078
11. Crawford DE, Porcheddu A, McCalmont AS, Delogu F, James SL, Colacino E (2020) ACS Sustainable Chem Eng 8:12230–12238
12. Linden M, Hofmann S, Herman A, Ehler N, Bär RM, Waldvogel SR (2023) Angew Chem Int Ed 62. https://doi.org/10.1002/anie.202214820
13. Yang M, Jiang R, Mu Y, Hong Y, Wan Y, Hou J, Tang D (2023) Chem Commun 59:2303–2306
14. Khan I, Rehman W, Rahim F, Hussain R, Khan S, Rasheed L, Alanazi MM, Alanazi AS, Abdellattif MH (2023) ACS Omega 8:22508–22522
15. Shayegan N, Haghipour S, Tanideh N, Moazzam A, Mojtabavi S, Faramarzi MA, Irajie C, Parizad S, Ansari S, Larijani B, Hosseini S, Iraji M, Mahdavi, M (2023) Sci Rep 13. https://doi.org/10.1038/s41598-023-32889-7
16. Zhao X-J, Xue L-W, Liu Q-R (2023) ACSi 70:524–532
17. Gupta S, Pandey SK, Kumar S, Gautam RN, Patel AK, Bharty MK, Kushwaha D, Acharya A, Butcher RJ (2023) J Mol Struct 1293:136212
18. Badawi WA, Samir M, Fathy HM, Okda TM, Noureldin MH, Atwa GMK, AboulWafa OM (2023) Bioorg Chem 138:106610
19. Burgos-López Y, Balsa LM, Piro OE, León IE, García-Tojal J, Echeverría GA, González-Baró AC, Parajón-Costa BS (2022) Polyhedron 213:115621
20. Wang L-H, Qiu X-Y, Liu S-J (2019) J Coord Chem 72:962–971
21. Kendur U, Chimmalagi GH, Patil SM, Gudasi KB, Frampton CS, Mangannavar CV, Muchchandi IS (2018) J Mol Struct 1153:299–310
22. Tiago FS, Santiago PHO, Amaral MMP, Martins JBL, Gatto CC (2015) J Coord Chem 69:330–342
23. Shit S, Chakraborty J, Samanta B, Slawin AMZ, Gramlich V, Mitra S (2009) Struct Chem 20:633–642
24. Mahmoudi G, Zaręba JK, Bauzá A, Kubicki M, Bartyzel A, Keramidas AD, Butusov L, Mirosław B, Frontera A (2018) Cryst Eng Comm 20:1065–1076
25. Mahmoudi G, Chowdhury H, Lofland SE, Ghosh BK, Kirillov AM (2017) J Coord Chem 70:1973–1983
26. Mao P-D, Sun H-Y, Yan F-F, Zhang S-H, Li X-F, Zhou R-H, Zhang Y-Q, Meng Y-S, Liu T (2023) CrystEngComm 25:6030–6038
27. Wu D-Y, Huang W, Wu G-H (2010) J Coord Chem 63:2976–2984
28. He Z, He C, Wang ZM, Gao EQ, Liu Y, Yan CH (2004) Dalton Trans 502. https://doi.org/10.1039/b315281b
29. Megger DA, Rosowski K, Radunsky C, Kösters J, Sitek B, Müller J (2017) Dalton Trans 46:4759–4767
30. Palepu NR, Premkumar JR, Verma AK, Bhattacharjee K, Joshi SR, Forbes S, Mozharivskyj Y, Rao KM (2018) Arab J Chem 11:714–728
31. Bjelogrlić SK, Todorović TR, Kojić M, Senćanski M, Nikolić M, Višnjevac A, Araškov J, Miljković M, Muller CD, Filipović NR (2019) J Inorg Biochem 199:110758
32. Ribeiro N, Correia I (2024) Front Chem Biol 3:1398873
33. Thirunavukkarasu T, Sparkes HA, Gandin V, Marzano C, Bertani R, Mozzon M, Scettri A, Albinati A, Demartin F, Casella G, Ferrante F, Zoleo A, Sgarbossa P, Natarajan K (2024) Inorg Chim Acta 566:122022
34. Vijayapritha S, Viswanathamurthi P, Vijayan P (2023) Inorg Chim Acta 553:121523
35. Richardson DR, Becker E, Bernhardt PV (1999) Acta Crystallogr C Cryst Struct Commun 55:2102–2105
36. Yang J, Liao G, Liu X, Zhao S, Yang Z (2022) J Inorg Biochem 236:111941
37. Bernhardt PV, Chin P, Sharpe PC, Richardson DR (2007) Dalton Trans 30:3232
38. Afkhami FA, Khandar AA, Mahmoudi G, Amini M, Molins E, Garczarek P, Lipkowski J, White JM, Kirillov AM (2017) Inorg Chim Acta 458:68–76
39. Mahmoudi G, Afkhami FA, Khandar AA, White JM, Maniukiewicz W, Babashkina MG, Mitoraj MP, Sagan F, Safin DA (2022) Cryst Eng Comm 24:3741–3748
40. Armstrong CM, Bernhardt PV, Chin P, Richardson DR (2003) Eur J Inorg Chem 2003:1145–1156
41. Zhao L, Wang J, Wu P, He C, Guo X, Duan C (2017) Sci Rep 7. https://doi.org/10.1038/s41598-017-18013-6
42. Li Z-W, Wang X, Wei L-Q, Ivanović-Burmazović I, Liu G-F (2020) J Am Chem Soc 142:7283–7288
43. Anwar MU, Dawe LN, Parsons SR, Tandon SS, Thompson LK, Dey SK, Mereacre V, Reiff WM, Bunge SD (2014) Inorg Chem 53:4655–4668
44. Kabsch W (2010) XDS. Acta Cryst D66:125–132
45. Bruker (2019) APEX3 Software, Bruker AXS Inc. v2019.11–0, Madison, Wisconsin, USA
46. Sheldrick GM (1997) SADABS. University of Goettingen, Germany, Program for Empirical Absorption Correction of Area Detector Data
47. Sheldrick GM (2008) Acta Crystallogr A Found Crystallogr A 64:112–122
48. Spek AL (2015) Acta Crystallogr C 71:9–18
49. Brandenburg K, Putz H (1999) DIAMOND. Crystal Impact GbR, Bonn, Germany
50. Brese NE, O'Keeffe M (1991) Acta Crystallogr B 47:192–197
51. Bernhardt PV, Wilson GJ, Sharpe PC, Kalinowski DS, Richardson DR (2008) J Biol Inorg Chem 13:107–119
52. Frisch MJ, Trucks GW, Schlegel J, Scuseria GE, Robb MA, Cheeseman JR, Schlegel HB, Scalmani G, Barone V, Mennucci B, Petersson GA (2010) Gaussian 09, Revision C.01. Gaussian, Inc., Wallingford, CT
53. Lu T, Chen F (2011) J Comput Chem 33:580–592
54. Bader RFW (1991) Chem Rev 91:893–928
55. Kashina MV, Kinzhalov MA, Smirnov AS, Ivanov DM, Novikov AS, Kukushkin VYu (2019) Chem Asian J 14:3915–3920
56. Bikbaeva ZM, Novikov AS, Suslonov VV, Bokach NA, Kukushkin VYu (2017) Dalton Trans 46:10090–10101
57. Baykov SV, Mikherdov AS, Novikov AS, Geyl KK, Tarasenko MV, Gureev MA, Boyarskiy VP (2021) Molecules 26:5672
58. Chupina AV, Shayapov V, Novikov AS, Volchek VV, Benassi E, Abramov PA, Sokolov MN (2020) Dalton Trans 49:1522–1530
59. Tskhovrebov AG, Novikov AS, Odintsova OV, Mikhaylov VN, Sorokoumov VN, Serebryanskaya TV, Starova GL (2019) J Organometall Chem 886:71–75
60. Manna P, Seth SK, Mitra M, Choudhury SR, Bauzá A, Frontera A, Mukhopadhyay S (2014) Cryst Growth Des 14:5812–5821
61. Mirzaei M, Eshtiagh-Hosseini H, Bolouri Z, Rahmati Z, Esmaeilzadeh A, Bauza A, Ballester P, Barceló-Oliver M, Mague JT, Notash B, Frontera A (2015) Cryst Growth Des 15:1351–1361
62. Mirdya S, Drew MGB, Chandra AK, Banerjee A, Frontera A, Chattopadhyay S (2020) Polyhedron 179:114374
63. Sharma P, Gogoi A, Verma AK, Frontera A, Bhattacharyya MK (2020) New J Chem 44:5473–5488
64. Chowhan B, Gupta M, Sharma N, Frontera A (2020) J Mol Struct 1207:127785

65. Kazmi M, Ibrar A, Ali HS, Ghufran M, Wadood A, Flörke U, Simpson J, Saeed A, Frontera A, Khan I (2019) J Mol Struct 1197:458–470
66. Bondi A (1966) J Phys Chem 70:3006–3007
67. Espinosa E, Molins E, Lecomte C (1998) Chem Phys Lett 285:170–173
68. Mikherdov AS, Kinzhalov MA, Novikov AS, Boyarskiy VP, Boyarskaya IA, Dar'in DV, Starova GL, Kukushkin VY (2016) J Am Chem Soc 138 :14129–14137
69. Mikherdov AS, Novikov AS, Kinzhalov MA, Boyarskiy VP, Starova GL, Ivanov AYu, Kukushkin VYu (2018) Inorg Chem 57:3420–3433
70. Mikherdov A, Novikov A, Kinzhalov M, Zolotarev A, Boyarskiy V (2018) Crystals 8:112
71. Siidra OI, Nazarchuk EV, Charkin DO, Chukanov NV, Zakharov AYu, Kalmykov SN, Ikhalaynen YA, Sharikov MI (2018) Zeitschrift Für Kristallographie - Crystalline Materials 234:109–118
72. Khrustalev VN, Grishina MM, Matsulevich ZV, Lukiyanova JM, Borisova GN, Osmanov VK, Novikov AS, Kirichuk AA, Borisov AV, Solari E, Tskhovrebov AG (2021) Dalton Trans 50:10689–10691
73. Espinosa E, Alkorta I, Elguero J, Molins E (2002) J Chem Phys 117:5529–5542
74. Johnson ER, Keinan S, Mori-Sánchez P, Contreras-García J, Cohen AJ, Yang W (2010) J Am Chem Soc 132:6498–6506
75. Contreras-García J, Johnson ER, Keinan S, Chaudret R, Piquemal J-P, Beratan DN, Yang W (2011) J Chem Theory Comput 7:625–632
76. Ringer AL, Senenko A, Sherrill CD (2007) Protein Sci 16:2216–2223
77. Rosokha SV (2023) Chem Plus Chem 88. https://doi.org/10.1002/cplu.202300350
78. Wang D-X, Wang M-X (2013) J Am Chem Soc 135:892–897
79. Groom CR, Bruno IJ, Lightfoot MP, Ward SC (2016) Acta Crystallogr B Struct Sci Cryst Eng Mater 72:171–179
80. Handy JV, Ayala G, Pike RD (2017) Inorg Chim Acta 456:64–75
81. Wei H, Qian J, Huang W, Zhang C (2016) J Clust Sci 27:1191–1201
82. Zhu H, Ströbele M, Yu Z, Wang Z, Meyer H-J, You X (2001) Inorg Chem Comm 4:577–581
83. Palion-Gazda J, Gryca I, Maroń A, Machura B, Kruszynski R (2017) Polyhedron 135:109–120
84. Machura B, Świtlicka A, Zwoliński P, Mroziński J, Kalińska B, Kruszynski R (2013) J Solid State Chem 197:218–227
85. Fan D, Yang CT, Ranford JD, Vittal JJ, Lee PF (2003) Dalton Trans 3376. https://doi.org/10.1039/b307610e
86. Shuku Y, Suizu R, Awaga K, Sato O (2009) Cryst Eng Comm 11:2065
87. Kose M, McKee V (2014) Polyhedron 75:30–39
88. Semenaka VV, Nesterova OV, Kokozay VN, Bon VV (2012) Acta Crystallogr E Struct Rep Online 68:m531–m532
89. Balić T, Đilović I (2024) Coord Chem Rev 518:216007
90. Lin Y-Z, Wu J-G, Xu G-X (1988) Mikrochim Acta 94:219–221